Advanced Studies in Pure Science and Applied Science

Chief Editor

Dr. B. M. Dhoot

Co-Editor

Dr. S.V. Kshirsagar

Dr. S.U. Kalme

Dr. P.R. Surve

Advanced Studies in Pure Science and Applied Science

Chief Editor
Dr. B. M. Dhoot

Co-Editor
Dr. S.V. Kshirsagar
Dr. S.U. Kalme
Dr. P.R. Surve

ISBN No. 978-93-82995-25-8

Published by:
Anuradha Publications
Cidco-Nanded

Publication Year: 2018-19

Price- Rs. 250/-

Printed by
Gurukrupa Offset,
Near Police Station, Gangakhed

Typesetting by:
Simran Computers
Gangakhed Dist.Parbhani

Cover Designby:
Mr. Imran K. Mohammad

CONTENTS

*****

Sol-gel synthesis and cation distribution of $Mg_{1-x}Zn_xFe_2O_4$ ferrite

Dr. Janardhan H. Shendkar
S. S. J. E S's
Arts, Commerce and Science College,
Gangakhed, Dist. Parbhani

Abstract

In the present work, preparation of $Mg_{1-x}Zn_xFe_2O_4$ ferrite carried out by sol-gel auto-combustion method at 80^oC to 100^oC and pH = 7. After heat treatment, X – ray diffraction pattern demonstrate formation of crystalline phase belonging to fcc system i.e. spinal crystal structure for every composition of MgZn ferrites. The average increase in the Lattice constant from $MgFe_2O_4$ to $ZnFe_2O_4$ is $0.053A^0$. The average particle size was 46 nm. The cation distribution shows it as mixed spinal ferrite. The divalent ion Zn^{2+} show stronger tetrahedral preference than Mg^{2+}, Mg^{2+} show stronger octahedral preference; while Fe^{3+} cation shows the (A)-site preference depending on the concentration of the Zn^{2+} cation in the composition and [B]- site preference on the concentration of the Mg^{2+} ions is the composition.

Keywords

Sol-gel auto-combustion, ferrite, cation, tetrahedral, octahedral

1. Introductions

A very important class of magnetic material is ferrimagnetic material called as ferrites. They have very large applications over the other magnetic materials. On account of its applications, ferrites are being studied since from (1952) last six decades for their basic properties such as structural, magnetic and electrical. Physicist and technologists have been prepared the ferrites by conventional ceramic method and non conventional methods, such as wet method i.e. co-precipitation organic precursors, co-spray roasting, freeze drying, fuel salt synthesis and sol-gel synthesis. Sol-gel processing provides a new approach to the preparation of ferrites. The advantage of the sol-gel method of synthesis is that virtually any, metal oxide system can be examined, and no special apparatus or equipment is required. Its advantages are the formation of ceramics of high purity and good control over microstructure and particle morphology in the synthesis typically at room temperature [1].

The main advantages of these low temperature processes are to give solid with large specific surface area and high porosity in the meso-pores and macro-pores range. The solid network is formed, from the solution via the hydrolysis and consideration of molecular precursors in solution [2]. The sol-gel process is a useful synthesis approach for the preparation of amorphous as well as structurally ordered materials. Through sol-gel process, it is possible to control the properties of the synthesized samples such as porosity and surface area to obtain homogenous matrices [3]. During the sol-gel process, the properties of the sol, the surface and pore structure of the support, the method of preparing gel membrane and its drying and firing conditions are the key factors influencing the pore structure and performance of membranes [4]. The sol-gel technique works well for the synthesis of complex metal oxides with high phase purity because the polymerizing gel traps the various metal ions components spatially, permitting precipitation from solution where all the metal ions occupy near neighbor position in the gel matrix, upon further processing and high temperature calcinations, the resultant amorphous mixture of metal oxides, hydroxides and metal salts decomposes with M-o-M bond formation.

Furthermore the gel matrix isolates the individual metal oxide particles, giving rise to nano structured grain after the high temperature calcinations to form the finished metal oxide [1]. Sol structures can, however, just as likely be more spectators in the crystallization process which form the final structures within gelled sol. Although sols may be formed as intermediate structures in some cases, they are clearly not necessarily transformed in to the primary particles or elementary structures, with in the gelled oxide [5]. Gel synthesis involves polymerizing molecular precursors into a three dimensional network and subsequently converting the wet gel in to a zero gel by removing the solvent [6]. In the sol gel route synthesis, a stepwise reaction scheme has been undertaken to control the ratios of hydrolysis to condensation rates. In general, the rate of hydrolysis is fast compared to that of condensation in strong acidic condition. Meanwhile, in neutral or basic conditions ranging from pH 7 to pH 8, the rate of condensation is faster than that of hydrolysis and eventually the material prepared by a single step reaction at high pH display gel-like structure with meso-pores [7].

1.1 Effect of variables on the sol-gel synthesis

The important variables are i) pH, ii) Water/metal alcoxide ratio, iii) Gelation temperature, iv) metal loading, v) addition of dopants and vi) solvent removal and

pretreatment condition [8]. In sol-gel synthesis, under strong acidic conditions (pH 1.5 - 6), hydrolysis occurred vary rapidly and gel formation time were increased substantially. In sol-gel synthesis, under base condition (pH 8-11), hydrolysis is slower and the polymerization is catalyzed by the base [9]. The reaction pH is very important in determining the final properties of the material which is synthesized.

i) Under basic conditions, the particles which are initially formed have a diameter of approximately 1 nm. These particles increase in size during the synthesis. The resultant gel tends to be meso-porous or macro-porous.
ii) When the reaction is performed at a pH of 7, the particles in the sol vary between 2.5 and 20 nm. For this the resultant gel has a non-uniform pore size.
iii) Under acid conditions the particles in both the sol and gel are very uniform. They vary in size between 0.5 and 3.0 nm and in general have very high porosities.

When non-stoichiometric amount of water were added, then from the analysis of the reaction products showed that; the extent of polymerization was largely depends on the number of molecules of water added [10]. When the H_2O alcoxide ratio is increased, the time required for formation of the gel is also observed to increase. An increase in the H_2O/ alcoxide ratio clearly leads to an increase in the pore diameter. When the H_2O / alcoxide ratio is close to that corresponding to stoichiometry, the surface area appears to go through a maximum [9]. In the sol-gel process, drying is regarded as an important procedure in the determination of the performance of the resultant zero-gels [10]. Among the many drying technique, thermal drying is employed most frequently for convenience, and a preceding ambient drying is usually performed. It is assumed that shortening the ambient drying period, along with shortening the total drying procedures, can tailor the characteristics of the resultant zero-gel [10].

2. Experimental techniques/methods of preparation

In sol gel auto-combustion method, A.R. grade metal nitrates i.e. ferric nitrate $Fe(NO_3)_3\ 9H_2O$, magnesium nitrate $Mg\ (NO_3)_2\ 6H_2O$, zinc nitrate $Zn\ (NO_3)_2\ 6H_2O$ (all are A, R. grade, s-define) were weighted according to the desired composition. As well as citric acid $C_6H_8O_7$ is weighted three times according to the desired composition. These weighted chemicals are dissolved in the non stoichiometric amount of distilled water. The mixtures were mixed by magnetic stirrer for 10 to 15 minutes at room temperature to get a well dissolved solution. A small amount of ammonia solution HNO_3

was added drop by drop to adjust the pH value of the solution about 7. After ½ hours of magnetic stirrer, it was obtained a viscous gel at 80°C to 100°C. With the continuation of heat at 100°C, after ½ hours, the non viscous gel was obtained first and then it was ignited. Therefore, sufficient amount of heat is produced the propagated reaction through the whole material. The combustion front (wave) spontaneously propagates and all the gel is burn out. After the completion of the exothermic reaction, large surface area and rich porous structure material with powder is obtained containing very fine crystallites due to rapid heating and cooling by the passage of the combustion wave front from the point of ignition through the solid material. The rapid moving combustion wave front, the high temperature and extremely high heating rate are some alterative features of the auto-combustion reaction.

The powder was grounded in agate martor for about ½ hours. All residual organic compounds were eliminated by heating the powder at 500°C in the air for 4 hours. Then, the calcinated powder was compacted and heat treated for 4 hours in an electric furnace at 450°C to 700°C to achieve a complete crystallization and controlled growth of crystallites.

2.1. X-ray diffraction

In the present work XRD pattern of the samples of the series was obtained on BRUKER AXS D8 advance x-ray diffractometer. The XRD patterns were recorded in the 2θ range of 20^0 to 80^0.

3. Results and Discussion

3.1. X-ray diffraction analysis

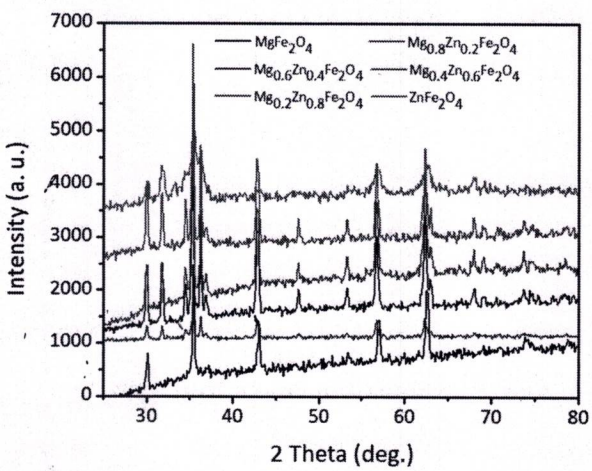

Fig. 3.1 The XRD pattern of $Mg_{1-x}Zn_xFe_2O_4$ ferrite

The XRD pattern of $Mg_{1-x}Zn_xFe_2O_4$ ferrite prepared by sol gel auto-combustion method and sintered at 600^{O}C are shown in Fig. 3.1. The patterns were indexed by applying Miller index Law. The values of Miller indices are obtained as (220), (311), (222), (400), (422), (511), (440) and (533). The values of h, k and l are obtained in every (hkl) are either even or odd, the results indicates that the material has well defined crystalline phase, belonging to the fcc system. The diffraction patterns gave a verification of the presence of spinel crystal structure for every composition of MgZn ferrites.

3.2. Lattice parameters

The results of the calculation of lattice constant (a) are presented in table 3.1. The values of Lattice parameter are calculated by using the formula [11].

Table 3.1

X	a (A^0)
0.0	8.400
0.2	8.443
0.4	8.448
0.6	8.447
0.8	8.448
1.0	8.453

$$a = \frac{\lambda}{2}\sqrt{\frac{N}{sin^2\theta}}$$

Where, $N = (h^2 + k^2 + l^2)$, θ = angle of diffraction, λ = wavelength of x-ray = 1.54 A^0

The value of Lattice parameter (a) varies from 8.400A^0 to 8.453A^0 with the addition of the Zn content in $Mg_{1-x}Zn_xFe_2O_4$. The lattice constant (a) is not increasing linearly with the addition of the Zn content as shown in Fig (3.2 (B)). The average increase in the Lattice constant from $MgFe_2O_4$ to $ZnFe_2O_4$ is 0.053A^0. It is observed that, the relation between the lattice constant (a) and composition (x) represent regions of 'variation' in Lattice parameter. There is a first phase of increase in lattice parameter (a), from the composition x=0 to x=0.2 with 81.13 % of the total increase. The second phase of increase in lattice parameter is from the composition x=0.2 to x=0.4, with 9.43 % of the total increase. The third phase of decrease in the lattice parameter is from composition x=0.4 to x=0.6 with, 1.88679 % with total increase. The fourth of increase in lattice

parameter is from composition x=0.6 to x=0.8 with 1.886789 % total increase. The fifth phase of increase in the Lattice parameter is from composition x=0.8 to x=1.0 with 9.43396 % of the total increase. This is shown in Table 3.2. This indicates that though the percent of dopant in the matrix of ferrite is controlled (+20 % each time), the percent increase in it is not uniform. This may be due to the fact that ferrite matrix (lattice) is sensitive to difference preparative parameters other than the percent of dopants.

Table 3.2

X	% increase in x	a (A^0)	% increase in a
0.0	20 %	8.400	+81.13%
0.2	20%	8.443	+9.43396%
0.4	20%	8.448	-1.88679%
0.6	20%	8.447	+1.88679%
0.8	20%	8.448	+9.43396%
1.0		8.453	
Total	100 %		100%

Thus with the increasing of the Zn content, on average there is increase in Lattice constant over total composition is observed, due to the cationic size effect. As, the cationic radius of Zn is greater than that of Mg, but the change in lattice parameter (a), from composition to composition is not linear. From the analysis the structure appears to be partially inversely which can be supported by the regularities and irregularities in the lattice constant with respect to composition (Vegards Law).

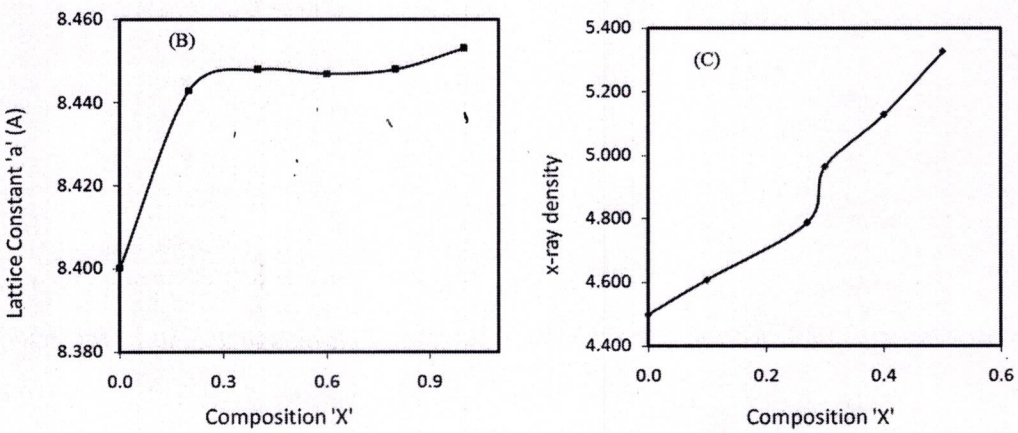

Fig. 3.2: (B) Plots of Lattice constant & Composition, (C) Plots of X-Ray Density & Composition.

3.3. X-ray density

The value of x-ray density d_x was calculated using the following formula [12].

$$d_X = \frac{8M}{Na^3}$$

Where 'M' 'N' and 'a' are the molecular weight, Avogadro's number and the lattice parameter respectively. The calculated values are presented in Table 3.3. The increase in x-ray density with addition of Zn element i.e. with composition is not linear as shown in fig. (3.2 (C)). The increase in x-ray density with composition (x) is due to replacement of Mg atoms by heavier Zn atom.

3.4. Average particle size (thickness)

The average particle size or thickness of the ferrite particles was determined from the full-width at half maximum of the most intense peak (311) using the well known Debye - Scherrer equation [13].

Table 3.3

X	dx (gm/cm³)	t (nm)
0.0	4.484	46.300
0.2	4.593	46.400
0.4	4.770	46.4000
0.6	4.953	46.4000
0.8	5.133	46.300
1.0	5.304	46.500

$$t = \frac{0.9\lambda}{B\ cos\theta_B}$$

Where, λ - x-ray wavelength, θ_B - the angle of Bragg diffraction, B - full width at half maximum.

Results of crystallite thickness estimated using Debye - Scheerer equation are given in Table (3.3). The particle size over all composition is almost constant; since the preparation was carried out under the same pH condition [9]. The average particle size was 46 nm.

3.5. Cation distribution

The cation distribution of Mg Zn ferrite system was obtained by x-ray diffraction method. The x-ray intensity of planes (220), (311), (222), (400), (511), (440) and (533) were calculated using the formula.

$$I = |F|^2 p L_p$$

Where, I - intensity of diffraction beam, F - structure factor, p - multiplicity factor and L_p - Lorentz polarization factor.

The calculated intensity ratio between the planes (222/511), (311/533) and (400/440) were compared with the observed intensity ratio between the same planes as in table (3.4).

Table 3.4

X	a (A^0)	d_{Ax} (A^0)	d_{Bx} (A^0)	d_{AxE} (A^0)	d_{BxE} (A^0) Shared	d_{BxE} (A^0) Unshared
0.0	8.400	1.878	2.023	3.066	2.785	2.934
0.2	8.443	1.880	2.025	3.070	2.789	2.937
0.4	8.448	1.882	2.027	3.073	2.791	2.940
0.6	8.447	1.884	2.029	3.076	2.794	2.943
0.8	8.448	1.885	2.031	3.079	2.797	2.946
1.0	8.453	1.888	2.034	3.083	2.801	2.950

Assuming that Zn^{2+} cations prefer to occupy only the A sites, while Mg^{2+} and Fe^{3+} cations were assuming to prefer both the A site and B site. The general formula for the cation distribution is given by

$$\left(Mg_y^{2+} Zn_x^{2+} Fe_{1-x-y}^{3+}\right)\left[Mg_{1-x-y}^{2+} Fe_{1+x+y}^{3+}\right]O_4$$

Where x and y represent the proportion of Zn^{2+} ion on A- site and Mg^{2+} ions on A site respectively.

The observed intensity ratio and calculated intensity ratio do not match exactly with each other. The cation distribution for which observed and calculated intensity ratio matches closely to each other is taken as the correct cations distribution and is shown in table (3.5).

The table (3.5) and (3.6) indicates that among the divalent ion Zn^{2+} show stronger tetrahedral preference than Mg^{2+}, due to their electronic configurations. Mg^{2+} show stronger octahedral preference; while Fe^{3+} cation shows the (A) - site preference depending on the concentration of the Zn^{2+} cation in the composition and [B] - site preference on the concentration of the Mg^{2+} ions is the composition.

Table 3.5

x	A-site	B-site	Intensity ratio			
			I_{311}/I_{533}		I_{400}/I_{440}	
			Cal	Obs.	Cal	Obs.
0	$Mg_0Zn_0Fe_1$	Mg_1Fe_1	1.65	1.43	1.819	0.85
	$Mg_{0.1}Zn_0Fe_{0.9}$	$Mg_{0.9}Fe_{1.1}$	1.63	1.43	0.998	0.85
	$Mg_{0.2}Zn_0Fe_{0.8}$	$Mg_{0.8}Fe_{1.2}$	1.62	1.43	0.367	0.85
	$Mg_{0.5}Zn_0Fe_{0.5}$	**$Mg_{0.5}Fe_{1.5}$**	**1.59**	**1.43**	**0.867**	**0.85**
			I_{222}/I_{511}		I_{400}/I_{440}	
			Cal	Obs.	Cal	Obs.
0.2	**$Mg_0Zn_{0.2}Fe_{0.8}$**	**$Mg_{0.8}Fe_{1.2}$**	**1.17**	**1.07**	**0.636**	**0.92**
	$Mg_{0.05}Zn_{0.2}Fe_{0.75}$	$Mg_{0.75}Fe_{1.25}$	0.87	1.07	0.66	0.92
	$Mg_{0.1}Zn_{0.2}Fe_{0.7}$	$Mg_{0.7}Fe_{1.3}$	0.60	1.07	0.88	0.92
0.4	**$Mg_0Zn_{0.4}Fe_{0.6}$**	**$Mg_{0.6}Fe_{1.4}$**	**0.95**	**1.06**	**0.644**	**0.92**
	$Mg_{0.05}Zn_{0.4}Fe_{0.55}$	$Mg_{0.55}Fe_{1.45}$	0.77	1.06	0.660	0.92
	$Mg_{0.01}Zn_{0.4}Fe_{0.5}$	$Mg_{0.5}Fe_{1.5}$	0.46	1.06	0.694	0.94
0.6	**$Mg_0Zn_{0.6}Fe_{0.4}$**	**$Mg_{0.4}Fe_{1.6}$**	**0.77**	**0.95**	**0.65**	**0.84**
	$Mg_{0.05}Zn_{0.6}Fe_{0.35}$	$Mg_{0.35}Fe_{1.65}$	0.49	0.95	0.67	0.84
	$Mg_{0.01}Zn_{0.6}Fe_{0.30}$	$Mg_{0.30}Fe_{1.7}$	0.35	0.95	0.699	0.84
0.8	**$Mg_0Zn_{0.8}Fe_{0.2}$**	**$Mg_{0.2}Fe_{1.8}$**	**0.63**	**1.07**	**0.66**	**0.95**
	$Mg_{0.05}Zn_{0.8}Fe_{0.15}$	$Mg_{0.15}Fe_{1.85}$	0.43	1.07	0.68	0.95
	$Mg_{0.01}Zn_{0.8}Fe_{0.1}$	$Mg_{0.1}Fe_{1.9}$	0.26	1.07	0.70	0.95
1.0	**$Zn_1Fe_{0.0}$**	**Mg_0Fe_2**	**0.50**	**1.10**	**0.68**	**0.87**

The values of the tetrahedral bond length (dAx) and octahedral bond length (dBx) are calculated using the formula given by equation

$$d_{Ax} = \left(u - \frac{1}{4}\right) a\sqrt{3}$$

$$d_{Bx} = a\sqrt{\left(3u^2 - \frac{11}{4}u + \frac{43}{64}\right)}$$

And the values of the shared and unshared edges are calculated by the formula given by equation

$$d_{AE} = \left(2u - \frac{1}{2}\right) a\sqrt{2}$$

$$(d_{BE})_{shared} = (1 - 2u)a\sqrt{2}$$

$$(d_{BE})_{unshared} = \sqrt{\left(4u^2 - 3u + \frac{11}{16}\right)}$$

These values of dAx, dBX, shared edges and unshared edges are shown in Table 3.4.

Table 3.6

x	A-site	B-site	Intensity ratio			
			I_{311}/I_{533}		I_{400}/I_{440}	
			Cal	Obs.	Cal	Obs.
0	$Mg_{0.5}Zn_0Fe_{0.5}$	$Mg_{0.5}Fe_{1.5}$	1.59	1.43	0.867	0.85
			I_{222}/I_{511}		I_{400}/I_{440}	
			Cal	Obs.	Cal	Obs.
0.2	$Mg_0Zn_{0.2}Fe_{0.8}$	$Mg_{0.8}Fe_{1.2}$	1.17	1.07	0.636	0.92
0.4	$Mg_0Zn_{0.4}Fe_{0.6}$	$Mg_{0.6}Fe_{1.4}$	0.95	1.06	0.644	0.92
0.6	$Mg_0Zn_{0.6}Fe_{0.4}$	$Mg_{0.4}Fe_{1.6}$	0.77	0.95	0.65	0.84
0.8	$Mg_0Zn_{0.8}Fe_{0.2}$	$Mg_{0.2}Fe_{1.8}$	0.63	1.07	0.66	0.95
1.0	$Zn_1Fe_{0.0}$	Mg_0Fe_2	0.50	1.10	0.68	0.87

4. Conclusions

1) With the increase of Zn^{2+} content on average there is increase in Lattice parameter over the total composition observed. But the variation in the lattice parameter from composition to composition is not linear.
2) The x-ray density increases with increase in the composition (x)
3) The particles have an average size 46 nm.
4) The cation distribution shows it as mixed spinel ferrite. The divalent ion Zn^{2+} show stronger tetrahedral preference than Mg^{2+}, Mg^{2+} show stronger octahedral preference; while Fe^{3+} cation shows the (A)-site preference depending on the concentration of the Zn^{2+} cation in the composition and [B]- site preference on the concentration of the Mg^{2+} ions is the composition.

References

1. J.Y. Ying, Nanostructured materials. Academic Press, (2001) 9-10.
2. J. Livage, Catalysis Today, (1998) 41:3-19.
3. R.F.D. Farias, U. Arnold, L. Martinez, U. Schechardt, M.J.D.M. Jannini, and C. Airoldi, Journal of Physics and Chemistry of Soils, (2003) 64:2384-2389.
4. X.S. Ju, P. Haung, N. P. Xu, and J. Shi, Journal of Membrane Science, (2000) 166:41-50.

5. L. L. Murrel, Catalysis Today, (1997) 35:225-245.
6. Y. Narender and D. L. Messing, Catalysis Today, (1997) 35:247-268.
7. D. G. Choi and S. M. Yang, Journal of Colloid and Interface Science, (2003) 261:127-132.
8. C.K. Lambert and R.D. Gonzalez, Journal of Solid State Chemistry, (2001) 158:154-161.
9. R.D. Ganzalez, T. Lopez, and R.Gomez, Catalysis Today, (1997) 35:293-317.
10. W.L. Hung, S. H. Chi, K. M. Liang, S. R. Gu, and Z. F. Yuan, Journal of Colloid and Interface Science, (2002) 246:129-134.
11. A.R. Varma and O.N. Srivastava, Crystallography Applied to solid state physics, New Age International Publishers.
12. B. D. Cullity, Elements of x-ray diffraction, Prentice Hall New York.
13. U. Battacharya and V.S. Dharshane, J. Mater Chem., (1995) 3:2.

****